This article has been accepted for publication in a future issue of this journal, but has not been fully edited. Content may change prior to final publication.

Action Recognition from One Example

Hae Jong Seo, *Student Member, IEEE,* and Peyman Milanfar, *Fellow, IEEE*

***Abstract*—We present a novel action recognition method based on space-time locally adaptive regression kernels and the matrix cosine similarity measure. The proposed method uses a single example of an action as a query to find similar matches. It does not require prior knowledge about actions; foreground/background segmentation, or any motion estimation or tracking. Our method is based on the computation of novel space-time descriptors from the query video, which measure the likeness of a voxel to its surroundings. Salient features are extracted from said descriptors and compared against analogous features from the target video. This comparison is done using a matrix generalization of the cosine similarity measure. The algorithm yields a scalar resemblance volume, with each voxel indicating the likelihood of similarity between the query video and all cubes in the target video. Using nonparametric significance tests by controlling the false discovery rate, we detect the presence and location of actions similar to the query video. High performance is demonstrated on challenging sets of action data containing fast motions, varied contexts, and complicated background. Further experiments on the Weizmann and KTH datasets demonstrate state-of-the-art performance in action categorization.**

***Index Terms*—Action Recognition, Space-time descriptor, correlation and regression analysis**

I. Introduction

A huge number of videos (e.g., BBC[1],Youtube[2]) are available online today and the number is rapidly growing. Human actions constitute one of the most important parts in movies, TV shows, and consumer-generated videos. Analysis of human actions in videos is considered a very important problem in computer vision because of such applications as human-computer interaction, content-based video retrieval, visual surveillance, analysis of sports events and more. The term "action" refers to a simple motion pattern as performed by a single subject, and in general lasts only for a short period of time, namely just a few seconds. *Action* is often distinguished from *activity* in the sense that action is an individual atomic unit of activity. In particular, human action refers to physical body motion. Recognizing human actions from video is a very challenging problem due to the fact that physical body motion can look very different depending on the context: for instance, similar actions with different clothes, or in different illumination and background can result in a large appearance variation; or, the same action performed by two different people may look quite dissimilar in many ways.

A. Problem Specification

We present a novel approach to the problem of human action recognition as a video-to-video matching problem. Here, recognition is generally divided into two parts: category classification and detection/ localization. The goal of action classification is to classify a given action query into one of several pre-specified categories (for instance, 6 categories from KTH action dataset [1]: boxing, hand clapping, hand waving, jogging, running, and walking). Meanwhile, action detection is meant to separate an action of interest from the background in a target video (for instance, spatiotemporal localization of a walking person). This paper tackles both action detection and category classification problems simultaneously by searching for an action of interest within other "target" videos with only a *single* "query" video. We focus on a sophisticated feature representation with an efficient and reliable similarity measure which also allows us to avoid the difficult problem of explicit motion estimation.

In general, the target video may contain actions similar to the query, but these will typically appear in completely different context (See Fig. 1 left.) Examples of such differences can range from rather simple optical or geometric differences (such as different clothes, lighting, action speed, scale, and view changes); to more complex inherent structural differences such as for instance a hand-drawn action video clip (e.g., animation) rather than a real human action.

B. Related work

Over the last two decades, many studies have attempted to tackle this problem and made impressive progress. Approaches can be categorized on the basis of *action representation*; namely, appearance-based representation [2], [3], [4], [5], shape-based representation [6], [7], [8], [9], optical-flow-based representation [10], [11], [12], [13], interest-point-based representation [1], [14], [15], [16], [17], [18], and volume-based representation [19], [20], [21], [22], [23], [24], [25]. We refer the interested reader to [26], [27], [28] and references therein for a good summary.

As examples of the interest-point-based approach which has gained a lot of interest, Niebles et al. [15], [14] considered videos as spatiotemporal bag-of-words by extracting space-time interest points and clustering the features, and then used a probabilistic Latent Semantic Analysis (pLSA) model to localize and categorize human actions. Yuan et al. [29] also used spatiotemporal features as proposed by [16]. They extended the naive Bayes nearest neighbor classifier [30], which was developed for object recognition, to action recognition. By modifying the efficient searching method based on branch-and-bound [31] for the 3-D case, they provided a very fast action detection method. However, the performance of these methods can degrade due to 1) the lack of enough training samples; 2) misdetections and occlusions of the interest points since they ignore global space-time information.

Shechtman and Irani [22] employed a three dimensional correlation scheme for action detection. They focused on

[1]http://www.bbcmotiongallery.com
[2]http://www.youtube.com

Digital Object Indentifier 10.1109/TPAMI.2010.156

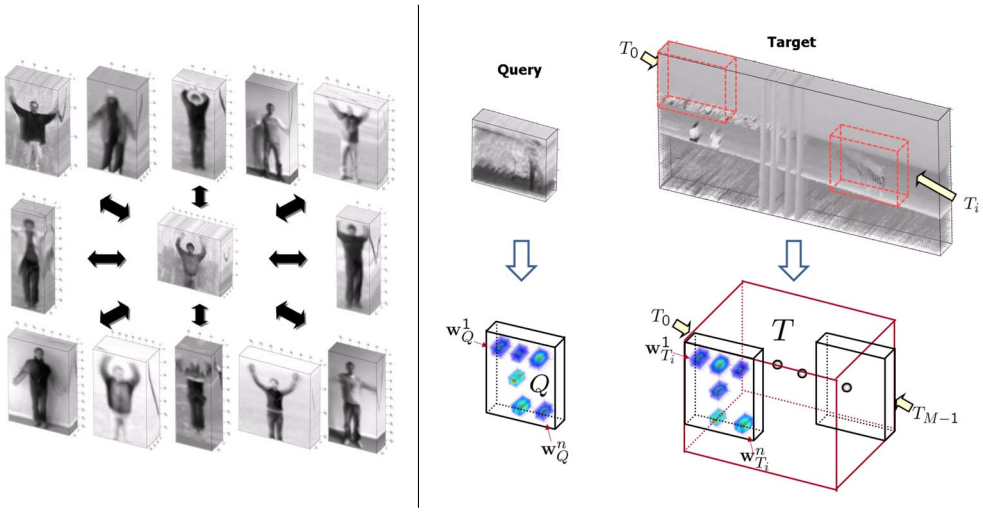

Fig. 1. Left: A hand-waving action and possibly similar actions, Right: Action detection problem (a) Given a query video Q, we wish to detect/localize actions of interest in a target video T. T is divided into a set of overlapping cubes (b) space-time local steering kernels (3-D LSKs) capture the space-time geometric structure of underlying data.

subvolume matching in order to find similar motion between the two space-time volumes, which can be computationally heavy. Ke et al. [23] presented an approach which uses boosting on 3-D Haar-type features inspired by similar features in 2-D object detection [32]. While these features are very efficient to compute, many examples are required to train an action detector in order to achieve good performance. They further proposed a part-based shape and flow matching framework [33] and showed good action detection performance in crowded videos. Recently, Kim et al. [24] generalized canonical correlation analysis to tensors and showed very good accuracy on the KTH action dataset, but their method requires a manual alignment process for camera motion compensation. Ning et al. [25] proposed a system to search for human actions using a coarse-to-fine approach with a five-layer hierarchical space-time model. These volumetric methods do not require background subtraction, motion estimation, or complex models of body configuration and kinematics. They tolerate variations in appearance, scale, rotation, and movement to some extent.

As opposed to 2-D object recognition which has recently proven capable of learning a respectably large number of categories (a couple of hundred), action recognition is still only limited to about a dozen categories at best (6 for the KTH, 10 for the Weizmann, and 12 for the Hollywood2 action dataset). Even though learning-based action recognition methods appear to be practical in a small number of categories, they have not yet proven to be scalable with a larger number of categories[3]. Thanks to the advent of large database-driven nonparametric approaches [34], [35], [36], instead of training sophisticated parametric models, we can reduce the inference problem to matching a query to an existing set of annotated databases, posing a video-to-video matching problem. As a successful example, Boiman et al. [30] showed that a rather simple nearest-neighbor (NN) based image classifier in the space of the local image descriptors is efficient and even outperforms the leading learning-based image classifiers such as SVM-KNN [37] and pyramid match kernel [38].

Methods such as those in [33], [22], [25], [39], [40] which aim at recognizing actions based solely on one query are very useful for applications such as video retrieval from the web (e.g., viewdle[4] and videosurf[5]). In these methods, a single query video is provided by users and every gallery video in the database is compared with the given query.

C. Overview of the Proposed Approach

In this paper, our contributions to the action recognition task are mainly two-fold. First, we propose a novel feature representation that is derived from space-time local (steering) regression kernels (3-D LSKs) which capture the underlying structure of the data quite well, even in the presence of significant distortions and data uncertainty. In fact, 3-D LSKs measure the likeness of a voxel to its surroundings based on computation of a distance between points measured (along the shortest path) on a manifold[6] defined by the embedding of the video data in 4-D as $[x_1, x_2, t, z(x_1, x_2, t)]$. Second, we generalize a training-free nonparametric detection scheme to 3-D, which we developed earlier for 2-D object detection [41]. We report state-of-the art performance on action category classification by using the resulting nearest neighbor classifier. In order to achieve better classification performance, we apply space-time saliency detection [42] to larger videos in order to automatically crop to a short action clip.

We propose to use 3-D LSKs for the problems of detection/localization of actions of interest between a query video and a target video as nicely formulated in [22] and also addressed in [40]. The key idea behind 3-D LSKs is to robustly obtain local space-time geometric structures by analyzing the radiometric (voxel value) differences based on estimated space-time gradients, and use this structure information to

[3]The heavy computational complexity of action recognition methods compared to object recognition is a possible reason, but the lack of large action recognition datasets covering many categories is the major impediment.

[4]http://www.viewdle.com
[5]http://www.videosurf.com
[6]See section II-A2 for details.

determine the shape and size of a canonical kernel (descriptor). The motivation to use these 3-D LSKs is the earlier successful work on adaptive kernel regression for image denoising, interpolation [43], deblurring [44], and superresolution [45]. The 3-D LSKs implicitly contain information about the local motion of the voxels across time, thus requiring no explicit motion estimation.

Referring to Fig. 2, by denoting the target video (T), and the query video (Q), we compute a dense set of 3-D LSKs from each. These densely computed descriptors are highly informative, but taken together tend to be over-complete (redundant). Therefore, we derive features by applying dimensionality reduction (namely PCA) to these resulting arrays, in order to retain the most salient characteristics of the 3-D LSKs. The feature collections from Q and T_i (a chunk of the target which is the same size as the query; See Fig. 1 right) form feature volumes $\mathbf{F}_Q$ and $\mathbf{F}_{T_i}$. We compare the feature volumes $\mathbf{F}_{T_i}$ and $\mathbf{F}_Q$ from the i^{th} cube of T and Q to look for matches. Inspired in part by many studies [46], [47], [48], [49], [50] which took advantage of cosine similarity over the conventional Euclidean distance, we employ *Matrix Cosine Similarity* (MCS) as a similarity measure which generalizes the notion of cosine similarity between two vectors [51], [52], [53]. The optimality properties of this approach are described in [41] within a naive Bayes framework.

In general, it is assumed that the query video is smaller than target video. However, this is not true in practice and a query video may indeed include a complex background which deteriorates recognition accuracy. In order to deal with this problem, it is necessary to have a procedure which automatically segments from the query video a small cube that only contains a valid human action. For this, we employ space-time saliency detection [42]. This idea not only allows us to extend the proposed detection framework to action category classification, but also improve both detection and classification accuracy by automatically removing irrelevant background from the query video. Fig. 2 shows an overview of our proposed framework for action detection.

[54] introduced a space-time local self-similarity descriptor for action detection and showed performance improvement over related earlier previous approach as [22]. It is worth mentioning that this (independently derived) local space-time self-similarity descriptor is a special case of 3-D LSK and is also related to a number of other local data adaptive metrics such as Optimal Space-Time Adaptation (OSTA) [55] and Non-Local Means (NLM) [56] which have been used very successfully for video restoration in the image processing community. A related, but different temporal self-similarity based descriptor [57] from [54] has been proposed for view-independent action recognition which shows good performance on action datasets such as the Weizmann [9] and the IXMAS [58], but they were not developed for action localization task.

As a related action representation, Ali and Shah [12] very recently proposed kinematic features (divergence, vorticity, symmetric and anti-symmetric optical flow and so forth) based on optical flows. By applying PCA to these features, they extracted dominant kinematic features and used them for action recognition along with the multiple instance learning approach

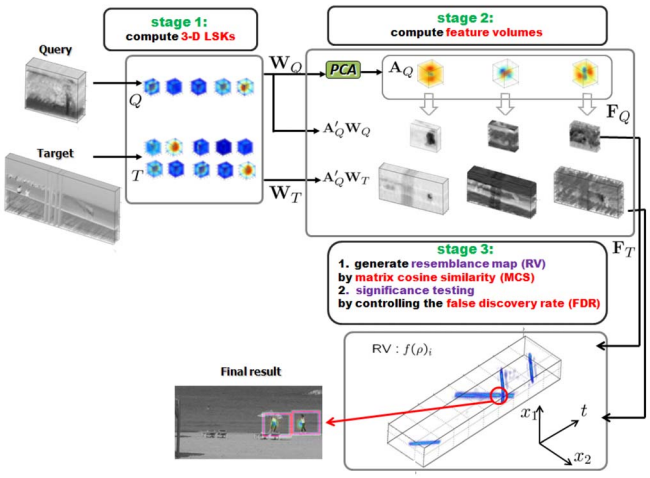

Fig. 2. System overview of action detection framework (There are broadly three stages.)

[59]. Our action representation is somewhat similar to theirs in the sense that we both use PCA to extract feature sets, but their method depends strongly on the number of (both positive and negative) training examples and explicitly estimates motion flows while our method uses a single query (positive example) for localization and our descriptors implicitly contain both shape and flow information at the same time. Very recently, [40] also made use of motion descriptors based on optical flows and focused on learning a distance function which is transferable to unseen action classes.

The proposed action detection method is distinguished from our earlier 2-D work in [41] proposed for object detection, in the following respects; 1) action detection addressed in this paper is considered to be more challenging than static (2-D) object detection due to additional problems such as variations in individual motion and camera motion, 2) we use space-time local steering kernels which capture both *spatial* and *temporal* geometric structure, 3) while [41] assumed that a query image is always smaller than a target and only contains an object of interest, we relax this assumption to deal with more realistic scenarios by incorporating space-time saliency detection [42], and 4) while [41] focused on detection tasks, in this paper, we further achieved state-of-the art action classification performance as well as high detection accuracy.

A preliminary version of this paper appeared in the IEEE International Conference on Computer Vision (ICCV '09) [60]. This paper is different from [60] in the following respects: 1) we provide more detailed description about what the proposed descriptors capture from video data, 2) we show that 3-D LSKs outperform simple linear 3-D Gabor filters and a state-of-the art 3-D descriptor called "HOG3D [61]" in our action detection framework by providing both quantitative and qualitative comparison results in Section III-A1, 3) a multi-scale approach is implemented to deal with large variations in scale of actions and is shown to outperform single-scale version in Section III-A1a, and 4) we test our method on more complicated and challenging dataset [62] for action localization.

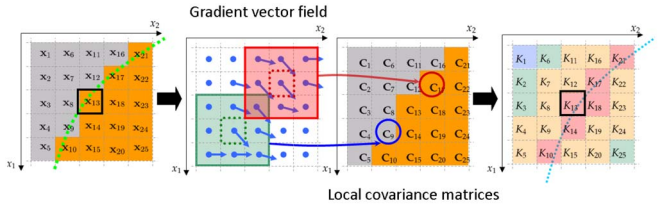

Fig. 3. Graphical description of how LSK values centered at pixel of interest $\mathbf{x}_{13}$ are computed in an edge region. Note that each pixel location has its own $\mathbf{C}_l \in \mathbb{R}^{2\times 2}$ computed from gradient vector field within a local window Ω_l (See green and red boxes). In K values, red means higher values (higher similarity).

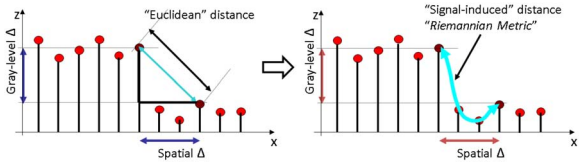

Fig. 4. LSK (right) captures distance between points measured along the shortest path on the image manifold whereas Bilateral kernel [63], Non-Local Means kernel [56], and Self-similarity kernel [54] (See left) are based on simple Euclidean distance.

II. Technical Details

As outlined in the previous section, our approach to detect actions consists broadly of three stages (see Fig 2.) Below, we describe each of these steps in detail. In order to make the concepts more clear, we first briefly describe the local steering kernels in 2-D. For extensive detail on this subject, we refer the reader to [43], [41].

A. Local Steering Kernel as a Descriptor

1) Local Steering Kernel in 2-D (LSK): The key idea behind LSK is to robustly obtain the local structure of images by analyzing the radiometric (pixel value) differences based on estimated gradients, and to use this structure information to determine the shape and size of a canonical kernel. The local steering kernel is defined as follows:

$$K(\mathbf{x}_l - \mathbf{x}_i) = \sqrt{\det(\mathbf{C}_l)} \exp\left\{ \frac{(\mathbf{x}_l - \mathbf{x}_i)^T \mathbf{C}_l (\mathbf{x}_l - \mathbf{x}_i)}{-2h^2} \right\}, \quad (1)$$

where $\mathbf{x}_i = [x_1, x_2]_i^T$ is a pixel of interest, $l = 1, \cdots, P$, $\mathbf{x}_l = [x_1, x_2]_l^T$ are a local neighboring pixels, h is a global smoothing parameter, P is the total number of samples in a local analysis window around a sample position at $\mathbf{x}_i$, and the matrix $\mathbf{C}_l \in \mathbb{R}^{(2\times 2)}$ is a covariance matrix estimated from a collection of first derivatives along spatial axes. More specifically, the covariance matrix $\mathbf{C}_l$ can be first naively estimated as $\mathbf{J}_l^T \mathbf{J}_l$ with

$$\mathbf{J}_l = \begin{bmatrix} \vdots & \vdots \\ z_{x_1}(\mathbf{x}_k), & z_{x_2}(\mathbf{x}_k) \\ \vdots & \vdots \end{bmatrix}, k \in \Omega_l, \quad (2)$$

where $z_{x_1}(\cdot)$ and $z_{x_2}(\cdot)$ are the first derivatives along x_1-, and x_2- axes and Ω_l is a local analysis window centered at $\mathbf{x}_l$. Fig. 3 illustrates how the covariance matrices and respective LSK values are computed.

At this point, it is useful to provide the reader with an interpretation of the information captured and represented by the LSK descriptors. Specifically, in order to measure the similarity of two pixels, in general, we can naturally consider both the spatial distance and the gray level distance (See Fig. 4). An effective way to combine these distances is to define a "signal-induced" distance or "Riemannian metric" [64] which basically stands for a distance between the points measure along the shortest path on the signal manifold. We can rewrite the matrix $\mathbf{C}_l$ as follows:

$$\mathbf{C}_l = \sum_{k\in\Omega_l} \begin{bmatrix} z_{x_1}^2(\mathbf{x}_k) & z_{x_1}(\mathbf{x}_k) z_{x_2}(\mathbf{x}_k) \\ z_{x_1}(\mathbf{x}_k) z_{x_2}(\mathbf{x}_k) & z_{x_2}^2(\mathbf{x}_k) \end{bmatrix}. \quad (3)$$

Then the term $(\mathbf{x}_l - \mathbf{x}_i)^T \mathbf{C}_l (\mathbf{x}_l - \mathbf{x}_i)$ in (1) is closely related to the Riemannian metric as:

$$\begin{aligned} &(\mathbf{x}_l - \mathbf{x}_i)^T \mathbf{C}_l (\mathbf{x}_l - \mathbf{x}_i) + (dx_1)_l^2 + (dx_2)_l^2 = \\ &\sum_{k\in\Omega_l} z_{x_1}^2(\mathbf{x}_k)(dx_1)_l^2 + 2 z_{x_1}(\mathbf{x}_k) z_{x_2}(\mathbf{x}_k)(dx_1)_l (dx_2)_l + \\ &z_{x_2}^2(\mathbf{x}_k)(dx_2)_l^2 + (dx_1)_l^2 + (dx_2)_l^2, \end{aligned} \quad (4)$$

where $(dx_1)_l = (x_1)_l - (x_1)_l$ and $(dx_2)_l = (x_2)_l - (x_2)_l$. See Appendix for details.

For the sake of robustness, we compute a more stable estimate of $\mathbf{C}_l$ by invoking the singular value decomposition (SVD) of $\mathbf{J}_l$ with regularization as [43], [41]

$$\mathbf{C}_l = \gamma \sum_{q=1}^{2} a_q^2 \mathbf{v}_q \mathbf{v}_q^T \in \mathbb{R}^{(2\times 2)}, \quad (5)$$

with

$$a_1 = \frac{s_1 + \lambda'}{s_2 + \lambda'}, \quad a_2 = \frac{s_2 + \lambda'}{s_1 + \lambda'}, \quad \gamma = \left(\frac{s_1 s_2 + \lambda''}{P}\right)^{\alpha}, \quad (6)$$

where λ' and λ'' are parameters[7] that dampen the noise effect and keep the denominators of a_q's from being zero, and α is a parameter [8] that restricts γ. The singular values (s_1, s_2) and the singular vectors $(\mathbf{v}_1, \mathbf{v}_2)$ are given by the compact SVD of $\mathbf{J}_l = \mathbf{U}_l \mathbf{S}_l \mathbf{V}_l^T = \mathbf{U}_l \mathrm{diag}[s_1, s_2]_l [\mathbf{v}_1, \mathbf{v}_2,]_l^T$. Note that $\sqrt{\det(\mathbf{C}_l)}$ in (1) plays a role as a general edge or corner indicator, thus giving higher weight to corresponding pixels. Since we use a robust estimate of $\mathbf{C}_l$, the LSKs reliably capture local geometry of the data manifold even in the presence of noise. The shape of the LSK's is not simply a Gaussian, despite the simple definition in (1) above. It is important to note that this is because for each pixel $\mathbf{x}_l$ in the vicinity of $\mathbf{x}_i$, a different matrix $\mathbf{C}_l$ is used, therefore leading to a far more complex and rich set of possible shapes for the resulting LSKs. Therefore, the LSKs can capture more sophisticated local geometry than histogram of gradients based descriptors such as SIFT and HOG which use locally quantized gradients information. The key idea explained above is equally valid in 3-D as well, as we describe below.

[7] λ' and λ'' are set to 1 and 10^{-8} respectively, and they are fixed for all experiments.

[8] α is set to 0.29 and fixed for all experiments.

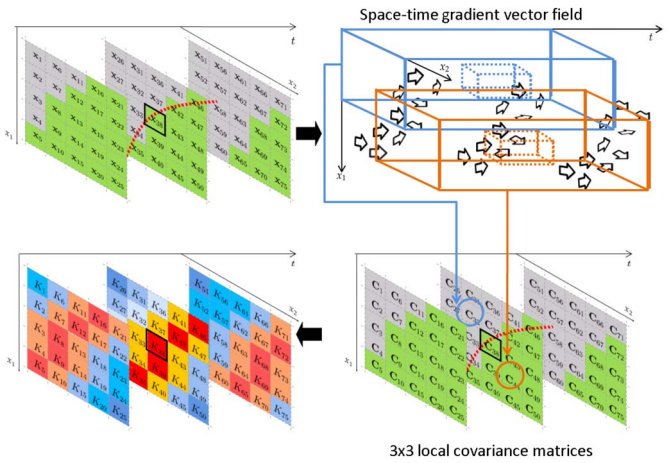

Fig. 5. Graphical description of how 3-D LSK values centered at voxel of interest $\mathbf{x}_{38}$ are computed in a space-time edge region. Note that each voxel location has its own $\mathbf{C}_l \in \mathbb{R}^{3\times 3}$ computed from space-time gradient vector field within a local space-time window.

2) Space-Time Local Steering Kernel (3-D LSK): Now, we introduce the time axis to the data model so that $\mathbf{x}_l = [x_1, x_2, t]_l^T$: x_1 and x_2 are the spatial coordinates, and t is the temporal coordinate. Similar to the 2-D case, the covariance matrix $\mathbf{C}_l$ can be naively estimated as $\mathbf{J}_l^T\mathbf{J}_l$ with

$$\mathbf{J}_l = \begin{bmatrix} \vdots & \vdots & \vdots \\ z_{x_1}(\mathbf{x}_k), & z_{x_2}(\mathbf{x}_k), & z_t(\mathbf{x}_k) \\ \vdots & \vdots & \vdots \end{bmatrix}, k \in \Omega_l \qquad (7)$$

where $z_{x_1}(\cdot), z_{x_2}(\cdot)$, and $z_t(\cdot)$ are the first derivatives along x_1-, x_2-, and $t-$ axes, and Ω_l is a *space-time* local analysis window (or cube) around a sample position at $\mathbf{x}_l$.

As explained in the 2-D LSK case, the term $(\mathbf{x}_l - \mathbf{x}_i)^T\mathbf{C}_l(\mathbf{x}_l - \mathbf{x}_i)$ in (1) now captures distance between the voxels measured along the shortest path on the embedded manifold of the video data. Fig. 5 illustrates how 3-D LSKs are computed in a space-time region. Again, $\mathbf{C}_l$ is estimated by invoking the singular value decomposition (SVD) of $\mathbf{J}_l$ with regularization as [45]:

$$\mathbf{C}_l = \gamma \sum_{q=1}^{3} a_q^2 \mathbf{v}_q \mathbf{v}_q^T \in \mathbb{R}^{(3\times 3)}, \qquad (8)$$

with

$$a_1 = \frac{s_1 + \lambda'}{\sqrt{s_2 s_3} + \lambda'},\ a_2 = \frac{s_2 + \lambda'}{\sqrt{s_1 s_3} + \lambda'},\ a_3 = \frac{s_3 + \lambda'}{\sqrt{s_1 s_2} + \lambda'},\ \gamma = \left(\frac{s_1 s_2 s_3 + \lambda''}{P}\right)^{\alpha} \qquad (9)$$

where λ' and λ'' are parameters[9] that dampen the noise effect and restrict γ and the denominators of a_q's from being zero. As mentioned earlier, the singular values (s_1, s_2, and s_3) and the singular vectors ($\mathbf{v}_1, \mathbf{v}_2$, and $\mathbf{v}_3$) are given by the compact SVD of $\mathbf{J}_l = \mathbf{U}_l\mathbf{S}_l\mathbf{V}_l^T = \mathbf{U}_l \text{diag}[s_1, s_2, s_3]_l [\mathbf{v}_1, \mathbf{v}_2, \mathbf{v}_3]_l^T$.

In the 3-D case, orientation information captured in 3-D LSK contains the motion information implicitly [45]. It is worth noting that a significant strength of using this implicit framework (as opposed to the direct use of estimated motion vectors) is the flexibility it provides in terms of smoothly and adaptively changing descriptors. This flexibility allows the accommodation of even complex motions, so long as their magnitudes are not excessively large[10].

[9] λ', λ'', and α are set to the same values as 2-D LSKs and fixed for all experiments.

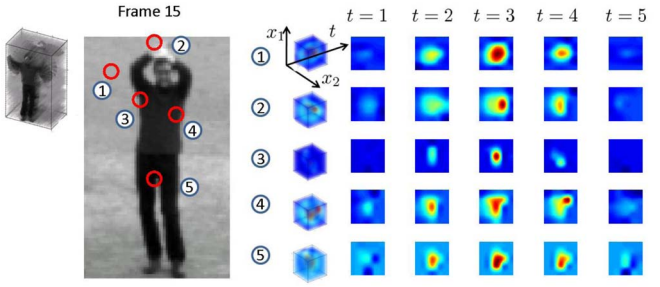

Fig. 6. Examples of 3-D LSKs capturing 3-D local underlying geometric structure in various regions. In order to compute 3-D LSKs, 5 frames (frame 13 to frame 17) were used. 3-D LSKs are shown upsampled for illustration only.

Fig. 6 shows examples of 3-D local steering kernels capturing 3-D local underlying geometric structure in various space-time regions. As can be seen in (1), the values of the kernel K are based on the covariance matrices $\mathbf{C}_l$ along with their space-time locations $\mathbf{x}_l$. Intuitively, $\mathbf{C}_l$'s computed from the local analysis window Ω_l are similar to one another in the motion-free region (see Fig. 6 [1]). On the other hand, in the region where motion exists (see Fig. 6 [2,3,4,5]), the kernel size and shape depend on both $\mathbf{C}_l$ and its space-time location $\mathbf{x}_l$ in the local space-time window. Thus, if the pixel of interest (center pixel of kernel) is located in space-time edge region, high values in the kernel are yielded along the space-time edge region whereas the rest of kernel values are near zero.

In what follows, at a position $\mathbf{x}_i$, we will essentially be using (a normalized version of) the function. $K(\mathbf{x}_l - \mathbf{x}_i)$ as descriptors, representing a video's inherent local space-time geometry. To be more specific, the 3-D LSK function $K(\mathbf{x}_l - \mathbf{x}_i)$ is densely calculated and normalized as follows

$$W_I^i = \frac{K(\mathbf{x}_l - \mathbf{x}_i)}{\sum_{l=1}^{P} K(\mathbf{x}_l - \mathbf{x}_i)}, \qquad (10)$$

where I can be Q or T for query or target, respectively[11]. Normalization of this kernel function yields invariance to brightness change and robustness to contrast change (as was similarly shown for 2-D LSKs in [41].)

Fig 7 shows that 3-D LSKs are effective at capturing local space-time geometry individually, and global space-time geometry collectively. It is interesting to note that 3-D LSKs[12] seem related to "HOG3D" introduced in [61]. However, our method is quite different in that our descriptors capture voxel relationships based on the locally measured distance between voxels using a natural signal induced metric, whereas HOG3D

[10] When the magnitude of the motions is large (relative to the support of the local steering kernels, specifically,) a basic form of coarse but explicit motion compensation will become necessary. We refer the reader to [45] for more detail.

[11] Note that videos here are gray scale. The case of color is worth treating independently and is discussed in [41]

[12] HoG [65] and HoF [66] are also related to our 2-D LSKs ($x_1 - x_2$ axes) and 2-D LSKs (either $x_1 - t$ axes or $x_2 - t$ axes).

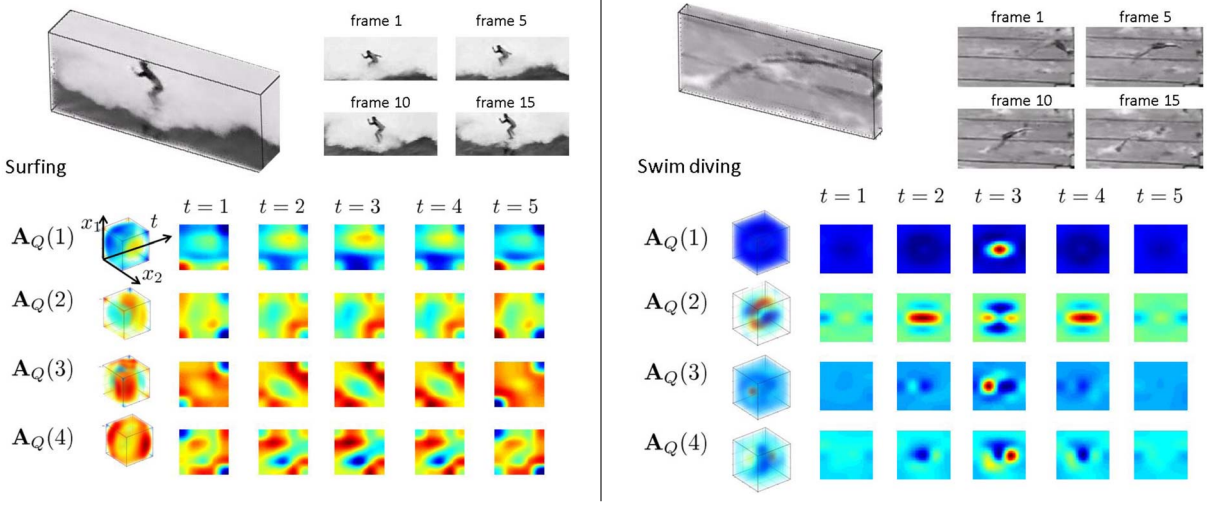

Fig. 8. Examples of top 4 principal components in $\mathbf{A}_Q$ for actions such as surfing and diving. Note that these eigenvectors reveal geometric characteristic of queries in both space and time domain, and thus they are totally different from linear 3-D Gabor filters. Eigenvectors $\mathbf{A}_Q$ were up-scaled for illustration

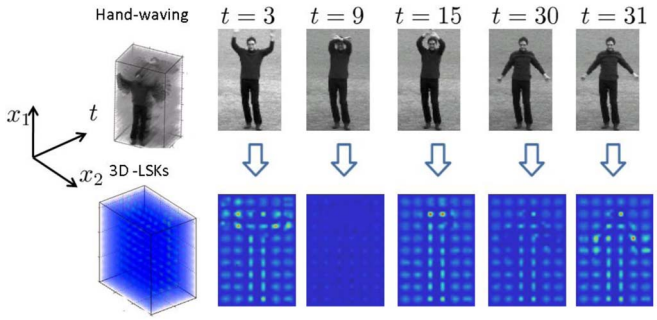

Fig. 7. 3D-LSKs computed from a hand-waving action are shown. For graphical description, we only computed 3-D LSKs at non-overlapping $5 \times 5 \times 5$ cubes, even though we compute 3-D LSKs densely in practice.

mostly makes use of the histogram of quantized local space-time gradients. Furthermore, we extract salient characteristics of 3-D LSKs by further applying Principal Component Analysis (PCA) as described in the following section. We believe that quantization of oriented gradients, while useful in reducing computational complexity, can lead to a significant degradation in discriminative power of descriptors. This effect is particularly severe in the case where there is only a single positive example available without any prior information, which we will explain in Section II.C. Superior performance of 3-D LSKs over HOG3D is demonstrated in Section III.A.

B. Feature representation

It has been shown in [41] that the normalized LSKs in 2-D follow a power-law (i.e., a long-tail) distribution. That is to say, the features are scattered out in a high dimensional feature space, and thus there basically exists no dense cluster in the descriptor space. The same principle applies to 3-D LSK. In order to illustrate and verify that the normalized 3-D LSKs also satisfy this property, we computed an empirical bin density (100 bins) of the normalized 3-D LSKs (using a total of $50,000$ 3-D LSKs) computed from 90 videos of the Weizmann action dataset [9] using the K-means clustering method. The utility of this observation becomes clear in the next paragraphs.

In the previous section, we computed a dense set of 3-D LSKs from Q and T. These densely computed descriptors are highly informative, but taken together tend to be over-complete (redundant). Therefore, we derive features by applying dimensionality reduction (namely PCA) to these resulting arrays, in order to retain only the salient characteristics of the 3-D LSKs. As also observed in [67], [30], an ensemble of local features with even little discriminative power can together offer significant discriminative power. However, both quantization and informative feature selection on a long-tail distribution can lead to a precipitous drop in performance. Therefore, instead of any quantization and informative feature selection, we focus on reducing the dimension of 3-D LSKs using PCA[13].

This idea results in a new feature representation with a moderate dimension which inherits the desirable discriminative attributes of 3-D LSK. The distribution of the resulting features sitting on the low dimensional manifold also tends to follow a power-law distribution and this allows us to the use *Matrix Cosine Similarity* (MCS) measure which will be illustrated in Section II-C. The optimality property and justification of MCS can be found in [41].

In order to organize W_Q and W_T, which are densely computed from Q and T, let $\mathbf{W}_Q$,$\mathbf{W}_T$ be matrices whose columns are vectors $\mathbf{w}_Q$,$\mathbf{w}_T$, which are column-stacked (rasterized) versions of W_Q,W_T respectively:

$$\mathbf{W}_Q = [\mathbf{w}_Q^1, \cdots, \mathbf{w}_Q^n] \in \mathbb{R}^{P \times n},$$
$$\mathbf{W}_T = [\mathbf{w}_T^1, \cdots, \mathbf{w}_T^{n_T}] \in \mathbb{R}^{P \times n_T}, \quad (11)$$

where n and n_T are the number of cubes where 3-D LSKs are computed in the query Q and the target T respectively.

As described in Fig. 2, the next step is to apply PCA to

[13] Ali and Shah [12] also pointed out that interest point descriptor-based action recognition methods have a limitation in that useful pieces of global information may be lost.

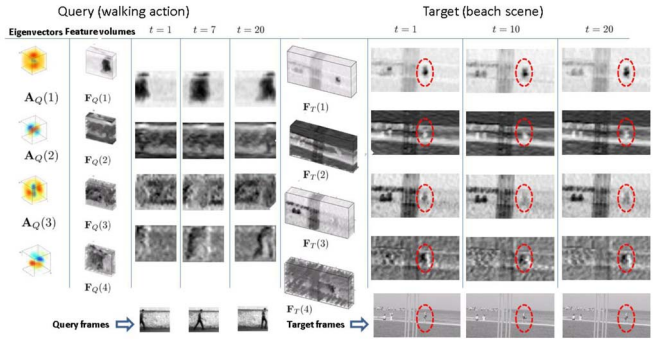

Fig. 9. $\mathbf{A}_Q$ is learned from a collection of 3-D LSKs $\mathbf{W}_Q$, and Feature row vectors of $\mathbf{F}_Q$ and $\mathbf{F}_T$ are computed from query Q and target video T respectively. Eigenvectors and feature vectors were transformed to volume and up-scaled for illustration purposes.

$\mathbf{W}_Q$ and retain the first (largest) d principal components[14] which form the columns of a matrix $\mathbf{A}_Q \in \mathbb{R}^{P\times d}$. Next, the lower dimensional features are computed by projecting $\mathbf{W}_Q$ and $\mathbf{W}_T$ onto $\mathbf{A}_Q$:

$$\mathbf{F}_Q = [\mathbf{f}_Q^1, \cdots, \mathbf{f}_Q^n] = \mathbf{A}_Q^T \mathbf{W}_Q \in \mathbb{R}^{d\times n},$$
$$\mathbf{F}_T = [\mathbf{f}_T^1, \cdots, \mathbf{f}_T^{n_T}] = \mathbf{A}_Q^T \mathbf{W}_T \in \mathbb{R}^{d\times n_T}. \quad (12)$$

Fig. 8 illustrate that the principal components $\mathbf{A}_Q$ learned from different actions such as surfing and diving actions are quite distinct from each other. Fig. 9 shows what the features $\mathbf{F}_Q, \mathbf{F}_T$ look like for a walking action. In order to show where actions appear, we drew red ovals around each action in the target video. These examples illustrate (as quantified later in the paper) that the derived feature volumes have a good discriminative power even though we do not involve any learning over a set of training examples.

It is worth noting that features derived from 3-D LSKs are not similar to 3-D Gabor filter responses. In fact, 3-D LSKs are highly non-linear but stable in the presence of uncertainty in the data while Gabor filters are linear and provide a fixed basis no matter what the given query. The Gabor representation may work reasonably well with supervised learning methods, but this does not necessarily mean that it is appropriate for the single-query framework of interest to us which we describe in the next section. We justify this points by showing both quantitative and qualitative comparison between 3-D LSK and 3-D Gabor filter responses in Section III-A1.

A similar approach was also taken by [68] where PCA was applied to interest point descriptors such as SIFT, leading to enhanced performance. Very recently, [12] proposed a set of kinematic features that extract different aspects of motion dynamics present in the optical flow. They obtained bags of kinematic modes for action recognition by applying PCA to a set of kinematic features. We differentiate our proposed method from [12] in the sense that 1) motion information is implicitly contained in 3-D LSK while [12] explicitly compute optical flow, 2) background subtraction was used as a pre-processing step, while our method is fully automatic, 3) [12] employed multiple instance learning for action classification while our proposed method deals with both action detection and classification from a single example.

[14]Typically, d is selected to be a small integer such as 3 or 4 so that 80 to 90% of the information in the LSKs would be retained. (i.e., $\frac{\sum_{i=1}^{d}\lambda_i}{\sum_{i=1}^{P}\lambda_i} \geq 0.8$ (to 0.9) where λ_i are the eigenvalues.)

C. Detecting Similar Actions using the Matrix Cosine Measure

1) Matrix Cosine Similarity: The next step in the proposed framework is a decision rule based on the measurement of a *distance* between the computed feature volumes $\mathbf{F}_Q, \mathbf{F}_{T_i}$. We were motivated by earlier works such as [50], [46], [47], that have shown the effectiveness of correlation-based similarity.

The *Matrix Cosine Similarity* (MCS) between two feature matrices $\mathbf{F}_Q, \mathbf{F}_{T_i}$ which consist of a set of feature vectors can be defined as the Frobenius inner product between two normalized matrices as follows:

$$\rho(\mathbf{F}_Q, \mathbf{F}_{T_i}) = <\overline{\mathbf{F}}_Q, \overline{\mathbf{F}}_{T_i}>_F = \text{trace}(\frac{\mathbf{F}_Q^T \mathbf{F}_{T_i}}{\|\mathbf{F}_Q\|_F \|\mathbf{F}_{T_i}\|_F}) \in [-1, 1], \quad (13)$$

where, $\overline{\mathbf{F}}_Q = \frac{\mathbf{F}_Q}{\|\mathbf{F}_Q\|_F} = \frac{1}{\|\mathbf{F}_Q\|_F}[\mathbf{f}_Q^1, \cdots, \mathbf{f}_Q^n]$ and $\overline{\mathbf{F}}_{T_i} = \frac{\mathbf{F}_{T_i}}{\|\mathbf{F}_{T_i}\|_F} = \frac{1}{\|\mathbf{F}_{T_i}\|_F}[\mathbf{f}_{T_i}^1, \cdots, \mathbf{f}_{T_i}^n]$. Equation (13) can be rewritten as a weighted sum of the vector cosine similarities $\rho(\mathbf{f}_Q, \mathbf{f}_{T_i}) = \frac{\mathbf{f}_Q^T \mathbf{f}_{T_i}}{\|\mathbf{f}_Q\| \|\mathbf{f}_{T_i}\|}$ ([50], [46], [47]) between each pair of corresponding feature vectors (i.e., columns) in $\mathbf{F}_Q, \mathbf{F}_{T_i}$ as follows:

$$\rho(\mathbf{F}_Q, \mathbf{F}_{T_i}) = \sum_{\ell=1}^{n} \frac{{\mathbf{f}_Q^\ell}^T \mathbf{f}_{T_i}^\ell}{\|\mathbf{F}_Q\|_F \|\mathbf{F}_{T_i}\|_F} = \sum_{\ell=1}^{n} \rho(\mathbf{f}_Q^\ell, \mathbf{f}_{T_i}^\ell) \frac{\|\mathbf{f}_Q^\ell\| \|\mathbf{f}_{T_i}^\ell\|}{\|\mathbf{F}_Q\|_F \|\mathbf{F}_{T_i}\|_F}. \quad (14)$$

The weights are represented as the product of $\frac{\|\mathbf{f}_Q^\ell\|}{\|\mathbf{F}_Q\|_F}$ and $\frac{\|\mathbf{f}_{T_i}^\ell\|}{\|\mathbf{F}_{T_i}\|_F}$ which indicate the relative importance of each feature in the feature sets $\mathbf{F}_Q, \mathbf{F}_{T_i}$. We see here an advantage of the MCS in that it takes account of the strength and angle similarity of vectors at the same time. Hence, this measure not only generalizes the cosine similarity naturally, but also overcomes the disadvantages of the conventional Euclidean distance which is sensitive to outliers[15].

It is worth noting that [22] proposed 3-D volume correlation score (global consistency measure between query and target cube) by computing a weighted average of local consistency measures. The difficulty with that method is that local consistency values should be explicitly computed from each corresponding subvolume of the query and target video. Furthermore, the weights to calculate a global consistency measure are based on a sigmoid function, which is somewhat ad-hoc. Here, we claim that our MCS measure is better motivated, more general, and effective than their global consistency measure for action detection as we also allude to in section III-A1.

[15]We compute $\rho(\mathbf{F}_Q, \mathbf{F}_{T_i})$ over M (a possibly large number of) target cubes and this can be efficiently implemented by column-stacking the matrices $\mathbf{F}_Q, \mathbf{F}_{T_i}$ and simply computing the (vector) cosine similarity between two long column vectors as follows:

$$\rho_i \equiv \rho(\mathbf{F}_Q, \mathbf{F}_{T_i}) = \sum_{\ell=1}^{n} \frac{{\mathbf{f}_Q^\ell}^T \mathbf{f}_{T_i}^\ell}{\|\mathbf{F}_Q\|_F \|\mathbf{F}_{T_i}\|_F}$$
$$= \rho(\text{colstack}(\mathbf{F}_Q), \text{colstack}(\mathbf{F}_{T_i})) \in [-1, 1],$$

where colstack$(\cdot)$ means an operator which column-stacks (rasterizes) a matrix.

The next step is to generate a so-called resemblance volume (RV), which will be a volume of voxels, each indicating the likelihood of similarity between the Q and T_i. As for the final test statistic comprising the values in the resemblance volume (as also described in [41]), we use the *proportion* of shared variance (ρ_i^2) to that of the "residual" variance ($1-\rho_i^2$). More specifically, RV is computed as follows[16]:

$$\text{RV} : f(\rho_i) = \frac{\rho_i^2}{1-\rho_i^2}. \tag{15}$$

The resemblance volume generated from $f(\rho_i)$ provides better contrast and dynamic range in the result ($f(\rho_i) \in [0, \infty]$). More importantly, from a quantitative point of view, we note that $f(\rho_i)$ is essentially the Lawley-Hotelling trace statistic [70], [71], which is used as an efficient test statistic for detecting correlation between two data sets. Furthermore, historically, this statistic has been suggested in the pattern recognition literature as an effective means of measuring the separability of two data clusters (e.g. [67].)

2) Significance Testing by Controlling the False Discovery Rate (FDR) [72]: If the task is to find the most similar cube (T_i) to the query (Q) in the target video, one can choose the cube which results in the largest value in the RV (i.e., $\max f(\rho_i)$) among all the cubes, no matter how large or small the value is in the range of $[0, \infty]$. This, however, is unwise because there may be no instances of the action of interest, or perhaps multiple actions of interest. Therefore, more generally, we are interested in multiple simultaneous hypotheses. We associate each voxel ($f(\rho_i)$) of the resemblance volume (RV) with a null hypothesis up to M hypotheses ($\mathcal{H}_0, \cdots, \mathcal{H}_{M-1}$) as:

$\mathcal{H}_0$:	T_0 is not similar to the given query Q	$\Leftrightarrow \quad f(\rho_0) < \tau$,
$\mathcal{H}_1$:	T_1 is not similar to the given query Q	$\Leftrightarrow \quad f(\rho_1) < \tau$,
$\vdots$	$\vdots$	$\vdots$
$\mathcal{H}_{M-1}$:	T_{M-1} is not similar to the given query Q	$\Leftrightarrow f(\rho_{M-1}) < \tau$.

where τ is a threshold for detection. Suppose that there are m_0 true null hypotheses among the M test hypotheses. Let R denote the number of hypotheses rejected. This observable random variable R can be decomposed as $V+S$, where V is the number of *incorrectly* rejected null hypotheses and S is the number of *correctly* rejected null hypotheses. The proportion of errors committed by falsely rejecting null hypotheses can be viewed through $\frac{V}{R}$. Let U be the unobservable random quotient,

$$U = \begin{cases} \frac{V}{R} & \text{if} \quad R > 0 \\ 0 & \text{otherwise.} \end{cases} \tag{16}$$

The false discovery rate (FDR) is defined as $\mathbf{E}(U)$, the expected error rate. The Benjamini-Hochberg procedure proposed in [72] controls the FDR at a desired level α, while maximizing $\mathbf{E}(R)$. Let $\{p_0, p_1, \cdots, p_{M-1}\}$ denote the p-values corresponding to the test statistics $\{f(\rho_0), f(\rho_1), \cdots, f(\rho_{M-1})\}$ and $p_{(0)} \leq p_{(1)} \leq \cdots \leq p_{(M-1)}$ denote the ordered p-values corresponding to the hypotheses $\{\mathcal{H}_{(0)}, \mathcal{H}_{(1)}, \cdots, \mathcal{H}_{(M-1)}\}$. By definition, $p_i = 1 - P_{\mathcal{H}_i}$ where $P_{\mathcal{H}_i}$ is the cumulative distribution function of resemblance volume under the null hypothesis $\mathcal{H}_i$. The FDR-controlling procedure is easily implemented. For the M voxels being tested, the general procedure is as follows:

1. Select a desired FDR bound α between 0 and 1. This is the maximum FDR that we are willing to tolerate on average.
2. Order the p values from the smallest to largest: $p_{(0)} \leq p_{(1)} \leq \cdots \leq p_{(M-1)}$ Let $f(\rho_{(i)})$ be the voxel corresponding to $p_{(i)}$.
3. Let γ be the largest i for which $p_{(i)} \leq \frac{i}{M}\alpha$
4. Identify the threshold τ corresponding to $p_{(\gamma)}$ and declare that the voxels of RV which is above τ contain similar actions to the given query Q.

After the significance testing with τ is performed, we employ the idea of non-maxima suppression [73] for the final detection. Namely, we take the volume region with the highest $f(\rho_i)$ score and eliminate the possibility that any other action is detected within some radius[17] of the center of that volume again. This enables us to avoid multiple false detections of nearby actions already detected. Then we iterate this process until the local maximum value falls below the threshold τ.

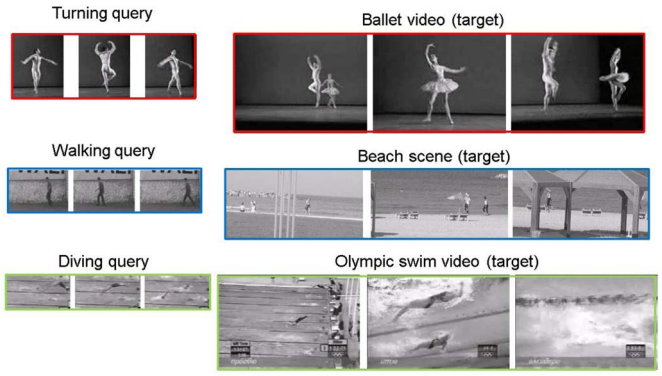

Fig. 10. Examples of general action dataset [22]: 1) a turning query and ballet video, a walking query and beach scene video, and a diving query and Olympic swim relay video.

III. Experimental Results

In this section, we demonstrate the performance of the proposed method with comprehensive experiments on four datasets: namely, the general action dataset [22], the drinking dataset, [62], the Weizmann action dataset [9], and the KTH action dataset [1]. The general action dataset and the drinking dataset are used to evaluate detection performance of the proposed method, while the Weizmann action dataset and the KTH action dataset are employed for action categorization. Comparison is made with state-of-the-art methods that have reported their results on these datasets.

[16]While the transformation is a monotonic function of the ρ statistic, its effect is not superfluous. Clearly, the distribution of $f(\rho)$ is different than that of ρ. Indeed, it is known that this transformation yields a new random variable which asymptotically approaches a fixed density: namely a squared Student-t variable, regardless of the density of the the input data [69]. Practically speaking, the usefulness of this transformation is in the fact that it normalizes the chosen threshold.

[17]The size of this exclusion region will depend on the application at hand and the characteristics of the query video.

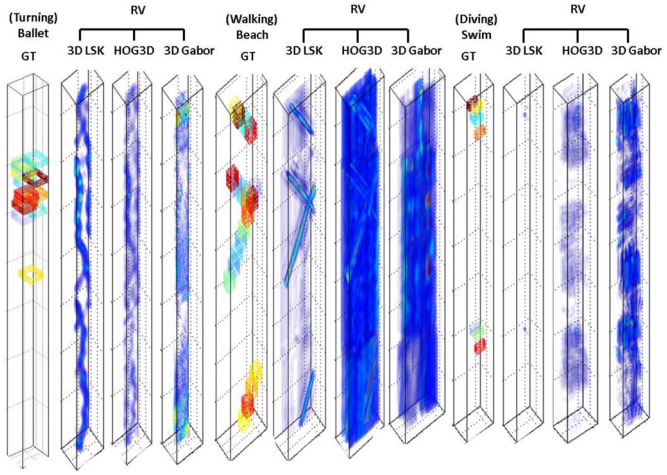

Fig. 11. Comparison of resemblance volumes (RV) among 3-D LSK, HOG3D, and 3-D Gabor for three pairs of videos (Ballet with a turning query, Beach with a walking query, and Swim with a diving query). HOG3D was computed densely for a fair comparison. Note that colors in the ground truth volume are used to distinguish individual actions from each other. This figure is better viewed in color.

A. Action Detection

In this section, we show several experimental results on searching with a short query video against a (typically longer and larger) target video. Our method detects the presence and location of actions similar to the given query and provides a series of bounding cubes with resemblance volume embedded around detected actions. Note again that no background/foreground segmentation and no explicit motion estimation are required in the proposed method. Our proposed method can also handle modest variations in rotation (up to ± 15 degree), and spatial and temporal scale change (up to $\pm 20\%$). For larger variations in scale, we use a multi-scale approach as similarly done in [41] and show in the following section that this results in improvement over the single-scale implementation.

Given Q and T, we spatially blur and downsample both Q and T by a factor of 3 in order to reduce the time-complexity. We then compute 3-D LSK of size 3×3 (space) $\times 7$ (time) as descriptors so that every space-time location in Q and T yields a 63-dimensional local descriptor $\mathbf{W}_Q$ and $\mathbf{W}_T$ respectively. The reason why we choose a lager time axis size than space axis of the cube is that we focus on detecting similar actions regardless of different appearances. Thus we give a higher priority to temporal evolution information than spatial appearance. We end up with $\mathbf{F}_Q$ and $\mathbf{F}_T$ by further reducing the dimension of descriptors[18] to d using PCA. Finally, we obtain RV by computing the MCS measure between $\mathbf{F}_Q$ and $\mathbf{F}_T$. After significance testing by controlling the FDR with a specified α value[19] and non-maxima suppression explained in Section II-C2, the proposed method localizes actions of interest[20].

[18]Note that $d = 4$ for the walking query whereas $d = 7$ for the ballet turning and diving queries.

[19]In our experiments, $\alpha = 0.01$ works well.

[20]The localization is considered to be correct when detected region is 50% overlapped with the ground truth.

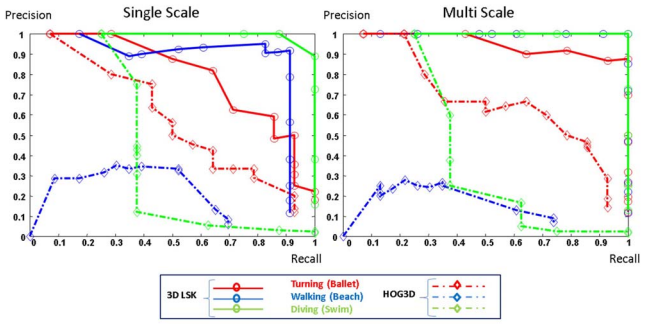

Fig. 12. Left: Comparison of Precision-Recall curves between 3-D LSK and HOG3D for three different actions (walking, ballet turning, and diving) in single-scale implementation Right: multi-scale comparision. Note that other state-of-the art action detection methods in [22], [54], [25] did not provide any quantitative performance on these examples. This figure is better viewed in color.

1) The General Action Dataset [54]: This dataset contains three pairs of action query and target videos. Note that the in all casses, the query video is not from the target video sequence.

a. The query video contains a single turn of a male dancer (13 frames of 90×110 pixels) while the target video (766 frames of 144×192 pixels) includes ballet actions from a male and a female dancers.
b. The query video contains a very short walking action moving to the left (14 frames of 60×70 pixels) with a stationary stone wall in the background while the target video has walking people in a beach scene (456 frames of 180×360 pixels) with crashing waves in the background.
c. The query video contains a swimmer's dive into a pool (16 frames of 70×140 pixels) while the target is an Olympic relay-match video (757 frames of 240×360 pixels) which was severely MPEG compressed.

As we alluded to in Section I-C, we compare our 3-D LSK with 3-D Gabor filter response [74] and HOG3D [61] both qualitatively and quantitatively[21]. Fig. 11 shows a comparison of resemblance volumes with 3-D LSK, HOG3D, and 3-D Gabor filter for three datasets. Note that we plugged in HOG3D and 3-D Gabor instead of 3-D LSK while the rest of the process in the proposed action detection framework remains exactly same. Red value in RVs signifies higher resemblance to the given query actions while blue means lower

[21]We set parameters for HOG3D and 3-D Gabor filters as follows:

1 HOG3D [61]: A 3-D patch of interest is divided into 3x3x2 space-time cells. The corresponding descriptor concatenates oriented gradient (10 orientations) histograms of all cells and is then normalized. With dense sampling (x_1x_2-stride: 6 pixels apart and t-stride:1 pixel apart), the resulting descriptors have 180 dimensions at every sampled position. We use the executable binary from the authors' website (downloadable from http://lear.inrialpes.fr/people/klaser/software_3d_video_descriptor. We set the parameters for this method to achieve its best performance. These parameters were not the same as those setting recommended at the website. This is because the recommended settings were not best suited for the general action dataset.)
2 3-D Gabor [74]: We used 16 of 3-D Gabor filter responses (0, $\pi/4$, $\pi/2$, $3\pi/4$: preferred direction of motion) and (1,2,3,4: preferred speed of the filter (in pixels per frame)). We use a matlab code from the website (downloadable from http://www.cs.rug.nl/~imaging/spatiotemporal_Gabor_function/GaborApp.html.)

Equal Error rate	3D LSK		HOG3D		3D Gabor	
	single	multi	single	multi	single	multi
(Turning) Ballet	**0.69**	**0.885**	0.5	0.656	0.09	0.286
(Walking) Beach	**0.91**	**1**	0.38	0.38	0	0
(Diving) Swim	**0.94**	**1**	0.34	0.26	0.25	0

Fig. 13. Comparison of equal error rates between 3-D LSK, HOG3D, and 3-D Gabor filter for three different actions (walking, ballet turning, and diving).

Equal Error rate	P = 3x3x7					h = 2.1			
	h=1.7	h=2.0	h=2.3	h=2.6	h=2.9	P = 3x3x5	P = 3x3x7	P = 5x5x5	P = 5x5x7
(Turning) Ballet	0.715	**0.725**	0.715	0.715	0.69	0.685	**0.74**	0.642	0.715
(Walking) Beach	0.853	0.915	**0.916**	0.876	0.88	0.93	**0.955**	0.82	0.915
(Diving) Swim	0.63	0.75	0.85	**0.94**	**0.94**	0.71	**0.8**	0.725	**0.8**

Fig. 14. Equal error rates with respect to different parameter settings on three datasets where equal error rate means a recall rate when a recall rate is the same as the precision rate.

resemblance. 3-D LSKs provide the most consistent results with the ground truth. We observe that RVs with 3-D LSKs reveal most relevant actions with a few false positives whereas HOG3D results in many false positives and 3-D Gabor filter misses most actions. It is worth noting that actions in target videos vary in scale. This can be better dealt with multi-scale approach as described below.

a) Multiscale Action Detection: We construct a multi-scale pyramid of the target feature volume $\mathbf{F}_T$. We resize the target feature volume size by steps of 10 %, so that a relatively fine quantization of spatial scales are taken into account. By using 5 scale factors from $0.9 \sim 1.3$, we obtain five resemblance volumes. These resemblance volumes represent the likelihood functions $p(f(\rho_i)|S_i)$ where S_i is the scale at $\mathbf{x}_i$. However the sizes of the respective resemblance volumes are naturally different. Therefore, we simply rescale all the resemblance volumes by voxel replication so that they match the dimensions of the original target volume. Next, the maximum likelihood estimate of the scale at each position is arrived at by comparing the rescaled resemblance volumes as follows[22]:

$$\hat{S}_i = \arg\max_{S_i} p(\underline{\mathrm{RV}}|S_i). \tag{17}$$

It is worth noting here that action detection methods [22], [54], [25] which also tested on this dataset only presented qualitative results with either empirically chosen threshold values or no description about how the threshold values are determined. On the other hand, the threshold values are automatically chosen in our algorithm by controlling the FDR with respect to the specified α. Unlike [22], [54], [25], we provide the precision-recall curves in Fig. 12 for quantitative evaluation. For these experiments, we used the entire frames while [22], [54], [25] used a part of video frames. The detection result

[22]By $\underline{\mathrm{RV}}$ we mean a collection of RV indexed by i at each position.

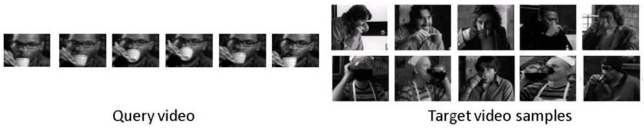

Fig. 15. The drinking dataset [62]: Left: a query video chosen from the episode "No problem". Right: Some target video samples from the episode "Cousin?" and "Delirium".

of the proposed method on this video outperforms those in [22], [25] and compares favorably to that in [54] in terms of visual detection accuracy. As shown in Figs. 12, 13 and expected from qualitative comparison in Fig. 11, 3-D LSK clearly outperforms HOG3D and 3-D Gabor.

b) Effect of Parameters: We examined how the performance of the proposed method is affected by the choice of parameters P (the size of 3-D LSK) and h (the smoothing parameter). Fig. 14 illustrates equal error rates for 3-D LSKs in single-scale implementation. As shown in Fig. 14, the overall performance of the proposed method changes gracefully with the particular choice of parameter h and P. It appears that best performance can be achieved with the fixed choice of $P = 3 \times 3 \times 7$ and $h = 2.3$ across three video dataset.

2) The Drinking Action Dataset [62]: In this section, we further evaluate our method on more challenging scenarios such as real movie scenes. The drinking action dataset comprises a total of 36,000 frames from two episodes of the movie "Coffee and Cigarette". The dataset includes 37 drinking actions from the episodes "Cousins?" and "Delirium". Fig. 15 (right) illustrates how drinking actions in target video samples largely vary in scales and view-points as well as the background clutter. Furthermore, there are abrupt scene changes, and the size and appearance of cups also vary. We chose one drinking action (55 frames of 107×101 pixels) as a query (see Fig. 15 (left)) from the episode called "No problem". Thus, there is no overlap between the query and the target videos. We take the multiscale approach in temporal axis as well as in spatial axis because temporal extents of drinking actions in the test set vary from 30 to 200 frames with the mean length of 70 frames. More specifically, we used 9 spatial scales from $0.7 \sim 1.5$ and 6 temporal scales from $0.8 \sim 1.3$. As explained in Section III-A1a, we take a maximum value across all scales at each voxel and end up with one RV. In order to deal with variations in view points, we used mirror-reflected version of the query as well. By voting the higher score among values from two RVs at every space-time location, we arrive at one RV which includes correct locations of drinking action. The performance of our method on this testset in comparison to Laptev's methods [62] is illustrated in Fig. 16 in terms of precision-recall curves and average precision (AP) values. Note that Laptev 1, 2, and 3 are based on discrete AdaBoost using 106 positive examples for training. As discussed in [62], Laptev 1 uses HOF with additional keyframe priming while Laptev 2 and 3 use HOG3D. Even though we use a single frontal view query, the proposed method performs favorably with Laptev 1 and 2. Twenty strongest detections (sorted in decreasing order of resemblance volume score) with the proposed method are

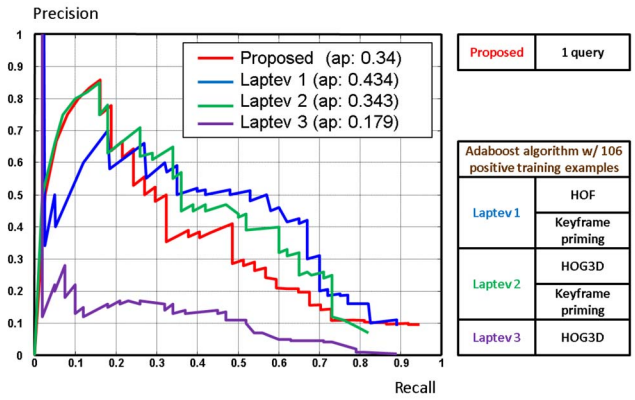

Fig. 16. Precision-Recall curves comparison between the proposed method and three action detection methods by [62]. The proposed method performs favorably with Laptev 1 and 2 even though there is a single query video used. The average precision (ap) means an average precision over the entire range

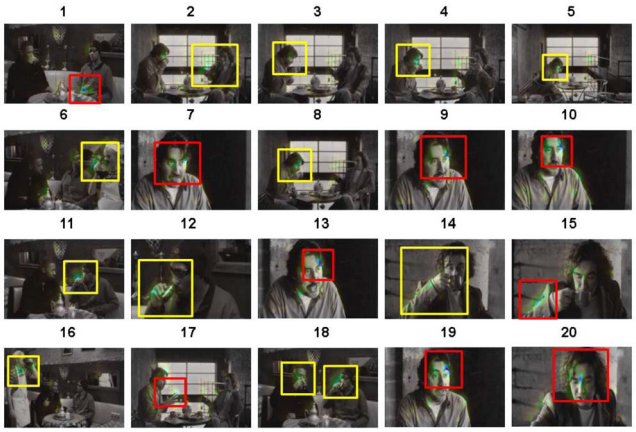

Fig. 17. Detection of drinking actions (yellow: true positives, red: false positives) sorted in the decreasing confidence order by the proposed method. This figure is better viewed in color.

illustrated in Fig. 17. In spite of a substantial variation in subject appearance, motion, surrounding scenes, view points and scales, and also abrupt scene change in the video, the proposed method retrieved most of actions at the correct locations. We expect that our method might also benefit from keyframe priming as discussed in [62].

B. Action Category Classification

As opposed to action detection, action category classification aims to classify a given action query into one of several pre-specified categories. In earlier discussion on action detection, we assumed that in general the query video is smaller than the target video. Now we relax this assumption, and thus we need a preprocessing step which selects a valid human action from the query video. This idea allows us not only to extend the proposed detection framework to action category classification, but also improves both detection and classification accuracy by removing unnecessary background from the query video.

Once the query video is cropped to a short action clip, the cropped query is searched against each labeled video in the database, and the value of the resemblance volume (RV) is viewed as the likelihood of similarity between the query and each labeled video. Then we classify a given query video

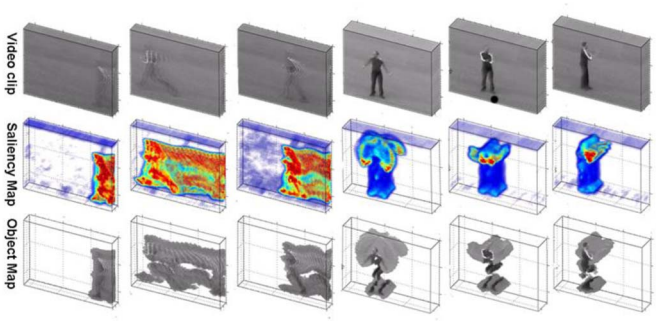

Fig. 18. Found space-time proto-objects from the KTH dataset [1]

as one of the predefined action categories using a nearest neighbor (NN) classifier.

1) Action Cropping in Videos: In this section, we introduce a procedure which automatically extracts from the query video a small cube that only contains a valid action. Space-time saliency detection [42] can provide such a mechanism. We downsample each frame of query video Q to a coarse spatial scale (64×64) in order to reduce the time-complexity[23]. We then compute 3-D LSK of size $3 \times 3 \times 3$ as features and generate feature matrices $\mathbf{F}_i$ in a $(3 \times 3 \times 7)$ local space-time neighborhood. We generated space-time saliency maps S by computing self-resemblance measure as shown in Fig. 18. Then, we use again the idea of non-parametric significance testing to detect space-time proto-objects. Namely, we compute an empirical PDF from all the saliency values and set a threshold by controlling FDR[24] with $\alpha = 0.05$ in deciding whether the given saliency values are in the extreme (right) tails of the empirical PDF. The approach is based on the assumption that in the video, a salient action is a relatively rare event and thus results in values which are in the tails of the distribution of saliency map values. After making a binary map by thresholding the space-time saliency map, a morphological filter is applied. More specifically, we dilate the binary object map with a disk shape of size 5×5. Proto-objects are extracted from corresponding locations of the original video. Fig. 18 shows that the space-time saliency detection method[25] successfully detects only salient human actions in the KTH dataset [1]. Next, we crop the valid human action region by fitting a 3-D rectangular box to space-time proto-objects.

2) The Weizmann Action Dataset [9]: The Weizmann action dataset contains 10 actions (bend, jumping jack, jump forward, jump in place, jump sideways, skip, run, walk, wave with two hands, and wave with one hand) performed by 9 different subjects. This dataset contains videos with static cameras and simple background, but it provides a good testing environment to evaluate the performance of the algorithm when the number of categories are large compared to the KTH dataset (a total of 6 categories). We conducted experiments on the Weizmann dataset under various data split setups. For example, the videos of m subjects are randomly drawn for

[23] We do not downsample the video in the time domain.

[24] We select a somewhat loose α level here since we do not wish to miss the relevant action in the query.

[25] We refer the reader to Fig. 19 in [42] for more challenging cases where background is very cluttered and moving as well.

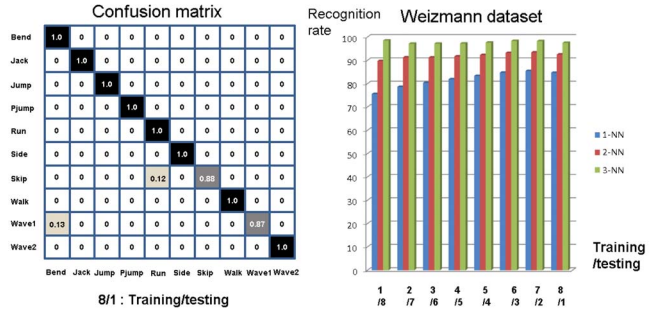

Fig. 19. Left: Confusion matrix on the Weizmann dataset for the leave-one-out setting, Right: Average recognition rate according to various data split setups. (Weizmann dataset)

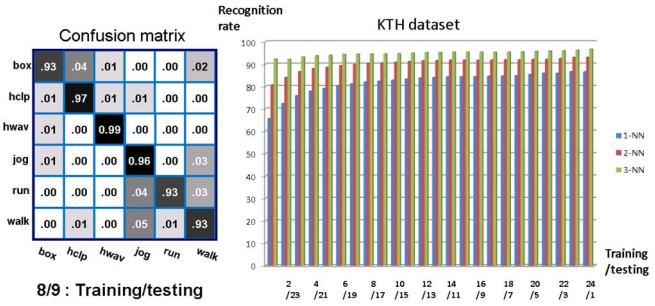

Fig. 20. Left: Confusion matrix on the KTH dataset for the 8 training/ 9 testing setup, Right: Average recognition rate according to different data split setup. (KTH dataset)

testing (query) and the videos of the remaining $9-m$ subject are labeled for each run where $m \in [1, \cdots, 8]$. We applied the automatic action cropping method introduced in the previous section to the query video. Then the resulting short action clip is matched against the remaining labeled videos using the proposed method. We classify each testing video as one of the 10 action types by 3-NN (nearest neighbor) as similarly done in [25]. The results are reported as the average of 100 runs. To begin, we achieved a recognition rate of 97.5% for all ten actions in the leave-one-out setting ($m = 1$). The recognition rate comparison is provided in Table I as well. The proposed method performs favorably against state-of-the-art methods [14], [57], [20], [75], [12], [76], [77], [61]. We observe that these results also compare favorably to several state-of-the-art methods even though our method involves no training phase, and requires no background/foreground segmentation. As an added bonus, our method provides localization of actions as a side benefit. Fig. 19 (left) shows the confusion matrix for our method.

TABLE I
COMPARISON OF AVERAGE RECOGNITION RATE ON THE WEIZMANN DATASET [9]

Our approach	3-NN	2-NN	1-NN
Recognition rate	**97.5%**	**92.5%**	**84.7%**

Method	Junejo et al. [57]	Liu et al. [20]	Klaser et al. [61]	Schindler and van Gool [78]
Recog. rate	95.33%	90%	84.3%	100%
Method	Niebles et al. [14]	Ali et al. [12]	Sun et al. [79]	Fathi and Mori [80]
Recog. rate	90%	95.75%	97.8%	100%
Method	Jhuang et al. [75]	Batra et al. [76]	Bregonzio et al. [81]	Zhang et al. [77]
Recog. rate	98.8%	92%	96.6%	92.89%

Next, we provide further results using 1-NN and 2-NN in comparison to 3-NN in Fig. 19 (right) with respect to various split setups. It is worth noting that the recognition rates are quite stable regardless of the split used.

3) The KTH Action Dataset [1]: In order to further quantify the performance of our algorithm, we also conducted experiments on the KTH dataset. The KTH action dataset contains six types of human actions (boxing, hand waving, hand clapping, walking, jogging, and running), performed repeatedly by 25 subjects in 4 different scenarios: outdoors (c_1), outdoors with camera zoom (c_2), outdoors with different clothes (c_3), and indoors (c_4). This dataset seems more challenging than the Weizmann dataset because there are large variations in human body shape, view angles, scales, and appearance. We also evaluate our method on the KTH dataset under various split setups. First, we use the same setup as in [1], *i.e.,* 8 people for training[26] and 9 for testing for each run. The recognition rates are reported as the average of 100 runs for this setup. We were able to achieve a recognition rate of 95.1% on these six actions. Fig. 20 (left) shows the average confusion matrix across all scenarios for this setup. The recognition rate comparison with competing methods is provided in Table II as well. It is worth noting that our method outperforms all the other state-of-the-art methods and is fully automatic. We further tried other data-split setups as similarly done in the previous section. The videos of m subjects are randomly drawn for testing (query) and the videos of the remaining subject $25-m$ are labeled for each run, where $m \in [1, \cdots, 24]$. As shown in Fig. 20 (right), it is consistent with the results on the Weizmann dataset that the recognition rates are quite stable regardless of the split used as similarly stated in [82].

TABLE II
COMPARISON OF AVERAGE RECOGNITION RATE ON THE KTH DATASET

Our approach	3-NN	2-NN	1-NN
Recognition rate	**95.1%**	**91%**	**82.7%**

Method	Kim et al. [24]	Ning et al. [25]	Klaser et al. [61]	Schindler [78] and van Gool [78]
Recog. rate	95.33%	92.31% (3-NN)	91.4%	92.7%
Method	Ali et al. [12]	Niebles et al. [14]	Liu and Shah [82]	Sun et al. [79]
Recog. rate	87.7%	81.5%	94.2%	94%
Method	Dollar et al. [83]	Wong et al. [84]	Rapantzikos et al. [85]	Laptev et al. [66]
Recog. rate	81.17%	84%	88.3%	91.8%

4) Discussion: It is important to note that our features computed using the PCA process are a function of the input query video, and therefore are adapted to each changing query. As such, one would expect them to serve better in identifying actions that are similar to the given query in a way that is more accurate than would a generic basis. Indeed, the tradeoff between having a fixed basis for all input queries and a basis that is extracted from each query manifests itself as a tradeoff between stability and specificity. Despite the higher computational cost we pay, our process for extraction of

[26]We use the term "training" here to be consistent with notation used in the literature even though our method does not require training mechanisms.

features appear to be stable, yet showing rather high specificity at the same time, resulting in overall very good performance.

Our system is designed with recognition accuracy as a high priority. A typical run of the action detection system implemented in Matlab takes a little over 1 minute on a target video T (50 frames of 144×192 pixels, Intel Pentium CPU 2.66 Ghz machine) using a query Q (13 frames of 90×110). Most of the run-time is taken up by the computation of MCS (about 9 seconds, and 16.5 seconds for the computation of 3-D LSKs from Q and T respectively, which needs to be computed only once.) There are many factors that affect the precise timing of the calculations, such as query size, complexity of the video, and 3-D LSK size. By applying coarse-to-fine search [86] or branch and bound [31] can be applied to speed up the method. As another way of reducing time-complexity, we could use look-up table instead of computing the local covariance matrix $\mathbf{C}$ at every pixel. Even though our method is stable in the presence of moderate amount of camera motion, our system can benefit from camera stabilization methods as done in [87], [88] in case of large camera movements.

In the Weizmann dataset and the KTH dataset, target videos contain only one type of action. However, target video may contain multiple actions in practice. In this case, simple nearest neighbor classifiers can possibly fail. Therefore, we might benefit from contextual information to increase accuracy of action recognition systems as similarly done in [89]. In fact, there is a broad agreement in the computer vision community about the valuable role that context plays in any image understanding task [90], [91].

IV. Conclusion and Future Directions

In this paper, we have proposed a novel action recognition algorithm by employing *space-time local steering kernels* which robustly capture underlying space-time data structure; and by using a training-free nonparametric detection scheme based on *Matrix Cosine Similarity*. The proposed method can automatically detect in the target video the presence, the number, as well as location of actions similar to the given query video by controlling the false discovery rate (FDR). Multi-scale implementation dealt with large variations in scale of actions and outperformed the single scale version. In order to increase the detection accuracy and further deal with action classification, we employed action cropping method based on space-time saliency detection. Challenging sets of real-world human action experiments demonstrated that the proposed approach achieves a high recognition accuracy and improves upon other state-of-the-art methods. Unlike most state-of-the-art methods that involve training, background/foreground segmentation, and manual aligning of actions, the proposed method operates using a *single* example of an action of interest to find similar matches; does not require any prior knowledge (learning) about actions being sought; and does not require any segmentation or pre-processing step of the target video.

The usefulness of 3-D LSK descriptors was justified for both action detection and recognition tasks in the example-based, single query detection scenario in Section III. It would be interesting to see how the proposed descriptors perform in comparison to state-of-the art 3-D descriptors such as HOG/HOF, HOG3, and etc; (see [92] and references therein) in other state-of-the art action recognition frameworks based on learning mechanisms [14], [12]. In case where a collection of negative action examples are available, we may be able to boost the action detection performance using "one-shot similarity (OSS) [93], [94]" kernel which was recently developed for face recognition task. Extending the proposed detection framework to joint learning from multiple queries would be an excellent direction which we intend to pursue in our future research. Since the proposed method is designed with detection accuracy as a high priority, extension of the method to a large-scale dataset requires a significant improvement of the computational complexity of the proposed method. Toward this end, we could benefit from an efficient searching method (coarse-to-fine search) and/or a fast nearest neighbor search method [27] (e.g., vantage point tree [97] and kernelized locality-sensitive hashing [98].)

Since local regression kernels in 2-D and in 3-D were originally designed for image (video) restoration, the proposed framework should become useful in jointly addressing the problems of enhancement and recognition where there might be a degraded query 1 target. By computing local regression kernels from images (video) at once, we may be able to not only detect objects (actions) of interest, but enhance images (videos) at the same time. These aspects of the work are the subject of ongoing research.

V. Appendix

Consider the parameterized surface $S(x_1, x_2) = \{x_1, x_2, z(x_1, x_2)\}$, embedded in the Euclidean space $\mathbb{R}^3$. The arclength on the surface is given by $ds^2 = dx_1^2 + dx_2^2 + dz^2$. Applying the chain rule, we have

$$dz(x_1, x_2) = \frac{\partial z}{\partial x_1} dx_1 + \frac{\partial z}{\partial x_2} dx_2 = z_{x_1} dx_1 + z_{x_2} dx_2. \quad (18)$$

Plugging $dz(x_1, x_2)$ into the arclength definition, we have

$$\begin{aligned} ds^2 &= dx_1^2 + dx_2^2 + dz^2 \\ &= dx_1^2 + dx_2^2 + (z_{x_1} dx_1 + z_{x_2} dx_2)^2 \\ &= (1 + z_{x_1}^2) dx_1^2 + 2 z_{x_1} z_{x_2} dx_1 dx_2 + (1 + z_{x_2}^2) dx_2^2 \end{aligned} \quad (19)$$

from which we can extract the metric coefficients

$$\begin{pmatrix} 1 + z_{x_1}^2 & z_{x_1} z_{x_2} \\ z_{x_1} z_{x_2} & 1 + z_{x_2}^2 \end{pmatrix} = \mathbf{C} + \mathbf{I}, \quad (20)$$

where $\mathbf{C}$ is the same covariance matrix in (3) and $\mathbf{I}$ is an identity matrix. In practice, the identity matrix here is absorbed in our calculation of $\mathbf{C}$ in the sense that we find a regularized estimate of $\mathbf{C}$.

VI. Acknowledgment

This work was supported in part by AFOSR Grant FA 9550-07-01-0365

[27] Note that in order for the fast nearest neighbor search method to be applicable, a generic basis such as sparse coding [95], [96] unlike query dependent PCA basis can be utilized at the expense of accuracy.

REFERENCES

[1] C. Schuldt, I. Laptev, and B. Caputo, "Recognizing human actions: A local SVM approach," *IEEE Conference on Pattern Recognition (ICPR)*, June 2004.

[2] T. Darrell and A. Pentland, "Classifying hand gestures with a view-based distributed representation," *In Advances in Neural Information Processing Systems*, vol. 6, pp. 945–952, 1993.

[3] J. Yamato, J. Ohya, and K. Ishii, "Recognizing human action in time sequential image using hidden markov model," *IEEE Conference on Computer Vision and Pattern Recognition (CVPR)*, 1992.

[4] H. Jiang, M. Crew, and Z. Li, "Successive convex matching for action detection," *IEEE Conference on Computer Vision and Pattern Recognition (CVPR)*, 2006.

[5] T. Starner and A. Pentland, "Visual recognition of American sign language using hidden Markov model," *International Workshop on Automatic Face and Gesture Recognition*, 1995.

[6] C. Carlsson and J. Sullivan, "Action recognition by shape matching to key frame," *Workshop on Models Versus Examplars in Computer Vision*, 2001.

[7] A. Yilmaz and M. Shah, "Actions sketch: A novel action representation," *IEEE Conference on Computer Vision and Pattern Recognition (CVPR)*, 2005.

[8] K. Cheung, S. Baker, and T. Kanade, "Shape-from-silhouette of articulated objects and its use for human body kinematics estimation and motion capture," *IEEE Conference on Computer Vision and Pattern Recognition (CVPR)*, 2003.

[9] L. Gorelick, M. Blank, E. Shechtman, M. Irani, and R. Basri, "Actions as space-time shapes," *IEEE Transactions on Pattern Analysis and Machine Intelligence (PAMI)*, vol. 29, no. 12, pp. 2247–2253, December 2007.

[10] A. F. Bobick and J. W. Davis, "The recognition of human movement using temporal templates," *IEEE Transactions on Pattern Analysis and Machine Intelligence (PAMI)*, vol. 23, no. 3, pp. 1257–1265, March 2001.

[11] J. Little and J. Boyd, "Recognizing people by their gait: The shape of motion," *Journal of Computer Vision Research*, 1998.

[12] S. Ali and M. Shah, "Human action recognition in videos using kinematic features and multiple instance learning," *Accepted for publication in IEEE Transactions on Pattern Analysis and Machine Intelligence (PAMI)*.

[13] Y. Yacoob and M. Black, "Parameterized modeling and recognition of activities," *Computer Vision and Image Understanding*, vol. 73, pp. 232–247, 1999.

[14] J. Niebles, H. Wang, and L. Fei-Fei, "Unsupervised learning of human action categories usig spatial-temporal words," *International Journal of Computer Vision (IJCV)*, vol. 79, no. 3, pp. 299–318, March 2008.

[15] J. Niebles and L. Fei-Fei, "A hierarchical models of shape and appearance for human action classification," *IEEE Conference on Computer Vision and Pattern Recognition (CVPR)*, June 2007.

[16] Z. Laptev and T. Lindeberg, "Space-time interest points," *IEEE International Conference on Computer Vision (ICCV)*, October 2003.

[17] I. Laptev, M. Marszalek, C. Schmid, and B. Rozenfeld, "Learning realistic human actions from movies," *IEEE Conference on Computer Vision and Pattern Recognition (CVPR)*, 2008.

[18] A. Oikonomopoulous, I. Patras, and M. Pantic, "Spatiotemporal saliency for human action recognition," *IEEE International Conference on Multimedia and Expo (ICME)*, 2005.

[19] T. Mahmood, A. Vasilescu, and S. Sethi, "Recognition of action events from multiple video points," *IEEE Workshop on Detection and Reconition of Events in Video, (ICCV)*, 2001.

[20] J. Liu, S. Ali, and M. Shah, "Recognizing human actions using multiple features," *IEEE Conference on Computer Vision and Pattern Recognition (CVPR)*, June 2008.

[21] P. Scovanner, S. Ali, and M. Shah, "A 3-dimensional SIFT descriptor and its application to action recognition," *ACM Multimedia*, 2007.

[22] E. Shechtman and M. Irani, "Space-time behavior-based correlation -orhow to tell if two underlying motion fields are similar without computing them?" *IEEE Transactions on Pattern Analysis and Machine Intelligence (PAMI)*, vol. 29, no. 11, pp. 2045–2056, November 2007.

[23] Y. Ke, R. Sukthankar, and M. Hebert, "Efficient visual event detection using volumetric features," *IEEE Conference on Computer Vision and Pattern Recognition (CVPR)*, 2005.

[24] T. Kim and R. Cipolla, "Canonical correlation analysis of video volume tensors for action categorization and detection," *IEEE Transactions on Pattern Analysis and Machine Intelligence*, vol. 31, no. 8, pp. 1415–1428, 2009.

[25] H. Ning, T. Han, D. Walther, M. Liu, and T. Huang, "Hierarchical space-time model enabling efficient search for human actions," *IEEE Transactions on Circuits and Systems for Video Technology*, vol. 19, no. 6, pp. 808–820, 2009.

[26] C. Cedras and M. Shah, "Motion based recognition: A survey," *Image and Vision Computing*, vol. 13, pp. 129–155, 1995.

[27] J. Aggarwal and Q. Cai, "Human motion analysis: A review," *Computer Vision and Image Understanding*, vol. 73, pp. 428–440, 1999.

[28] P. Turaga, R. Chellappa, V. Subrahmanian, and O. Udrea, "Machine recognition of human activities: A survey," *IEEE Transactions on Circuits and Systems for Video Technology*, vol. 18, no. 11, pp. 1473–1488, November 2008.

[29] J. Yuan, Z. Liu, and Y. Wu, "Discriminative subvolume seaerch for efficient action detection," *IEEE Conference on Computer Vision and Pattern Recognition (CVPR)*, 2009.

[30] O. Boiman, E. Shechtman, and M. Irani, "In defense of nearest-neighbor based image classification," *IEEE Conference on Computer Vision and Pattern Recognition (CVPR)*, 2008.

[31] C. H. Lampert, M. B. Blaschko, and T. Hofmann, "Beyond sliding windows: Object localization by efficient subwindow search," *IEEE Conference on Computer Vision and Pattern Recognition (CVPR)*, 2008.

[32] P. Viola and M. Jones, "Robust real-time object detection," *International Journal of Computer Vision (IJCV)*, vol. 57, no. 2, pp. 137–154, 2004.

[33] Y. Ke, R. Sukthankar, and M. Hebert, "Event detection in crowded videos," *IEEE International Conference on Computer Vision (ICCV)*, 2007.

[34] A. Torralba, R. Fergus, and W. Freeman, "80 million tiny images: a large dataset for non-parametric object and scene recognition," *IEEE Transcations on Pattern Analysis and Machine Intelligence (PAMI)*, vol. 30, no. 11, pp. 1958–1970, 2008.

[35] B. C. Russell, A. Torralba, K. P. Murphy, and W. T. Freeman, "LabelMe: a database and web-based tool for image annotation," *International Journal of Computer Vision (IJCV)*, vol. 77, no. 1-3, pp. 157–173, 2008.

[36] J. Hays and A. Efros, "Scene completion using millions of photographs," *ACM SIGGRAPH*, vol. 26, no. 3, 2007.

[37] H. Zhang, A. Berg, M. Maire, and J. Malik, "SVM-KNN: Discriminative nearest neighbor classification for visual category recognition," *IEEE Conference on Computer Vision and Pattern Recognition (CVPR)*, 2006.

[38] K. Grauman and T. Darrell, "The pyramid match kernel: Efficient learning with sets of features," *Journal of Machine Learning Research*, vol. 8, pp. 725–760, 2007.

[39] C. Yeo, P. Ahammad, K. Ramchandran, and S. S. Satry, "High-speed action recognition and localization in compressed domain videos," *IEEE Transactions on Circuits and Systems for Video Technology*, vol. 18, pp. 1006–1015, Aug 2008.

[40] W. Yang, Y. Wang, and G. Mori, "Human action recognition from a single clip per action," *2nd International Workshop on Machine Learning for Vision-based Motion Analysis, (ICCV)*, 2009.

[41] H. J. Seo and P. Milanfar, "Training-free, generic object detection using locally adaptive regression kernels," *To appear in IEEE Transactions on Pattern Analysis and Machine Intelligence*, 2010.

[42] ——, "Static and space-time visual saliency detection by self-resemblance," *The Journal of Vision,*, vol. 9(12), no. 15, pp. 1–27, 2009. [Online]. Available: http://journalofvision.org/9/12/15/,doi: 10.1167/9.12.15

[43] H. Takeda, S. Farsiu, and P. Milanfar, "Kernel regression for image processing and reconstruction," *IEEE Transactions on Image Processing (TIP)*, vol. 16, no. 2, pp. 349–366, February 2007.

[44] ——, "Deblurring using regularized locally-adaptive kernel regression," *IEEE Transactions on Image Processing (TIP)*, vol. 17, pp. 550–563, April 2008.

[45] H. Takeda, P. Milanfar, M. Protter, and M. Elad, "Super-resolution without explicit subpixel motion estimation," *IEEE Transactions on Image Processing (TIP)*, vol. 18, no. 9, pp. 1958–1975, September 2009.

[46] Y. Fu, S. Yan, and T. S. Huang, "Correlation metric for generalized feature extraction," *IEEE Transactions on Pattern Analysis and Machine Intelligence (PAMI)*, vol. 30, no. 12, pp. 2229–2235, 2008.

[47] Y. Fu and T. S. Huang, "Image classification using correlation tensor analysis," *IEEE Transactions on Image Processing (TIP)*, vol. 17, no. 2, pp. 226–234, 2008.

[48] C. Liu, "The Bayes decision rule induced similarity measures," *IEEE Transactions on Pattern Analysis and Machine Intelligence (PAMI)*, vol. 29, no. 6, pp. 1086–1090, 2007.

[49] D. Lin, S. Yan, and X. Tang, "Comparative study: Face recognition on unspecific persons using linear subspace methods," *IEEE International Conference on Image Processing (ICIP)*, 2005.

[50] Y. Ma, S. Lao, E. Takikawa, and M. Kawade, "Discriminant analysis in correlation similarity measure space," *IEEE International Conference on Machine Learning (ICML)*, 2007.

[51] J. W. Schneider and P. Borlund, "Matrix comparison, part 1: Motivation and important issues for measuring the resemblance between proximity measures or ordination results," *Journal of the American Society for Information Science and Technology*, vol. 58, no. 11, pp. 1586–1595, 2007.

[52] P. Ahlgren, B. Jarneving, and R. Rousseau, "Requirements for a cocitation similarity measure, with special reference to Pearson's correlation coefficient," *Journal of the American Society for Information Science and Technology*, vol. 54, no. 6, pp. 550–560, 2003.

[53] J. Rodgers and W. Nicewander, "Thirteen ways to look at the correlation coefficient," *The American Statistician*, vol. 42, no. 1, pp. 59–66, 1988.

[54] E. Shechtman and M. Irani, "Matching local self-similarities across images and videos," *IEEE Conference on Computer Vision and Pattern Recognition (CVPR)*, 2007.

[55] J. Boulanger, C. Kervrann, and P. Bouthemy, "Space-time adaptation for patch-based image sequence restoration," *IEEE Transactions on Pattern Analysis and Machine Intelligence (PAMI)*, vol. 29, pp. 1096–1102, June 2005.

[56] A. Buades, B. Coll, and J. M. Morel, "Nonlocal image and movie denoising," *International Journal of Computer Vision (IJCV)*, vol. 76, no. 2, pp. 123–139, 2008.

[57] I. N. Junejo, E. Dexter, I. Laptev, and P. Perez, "View-independent action recognition from temporal self-similarities," *To appear in IEEE Transations on Pattern Analysis and Machine Intelligence*, 2010.

[58] D. Weinland, E. Boyer, and R. Ronfard, "Action recognition from arbitrary views using 3d exemplars," *IEEE International Conference on Computer Vision (ICCV)*, 2007.

[59] Y. Chen, J. Bi, and J. Wang, "MILES: Multiple-instance learning via embedded instance selection," *IEEE Transcations on Pattern Analysis and Machine Intelligence (PAMI)*, vol. 28, no. 12, pp. 1931–1947, 2006.

[60] H. J. Seo and P. Milanfar, "Generic human action detection from a single example," *IEEE International Conference on Computer Vision(ICCV)*, Sep 2009.

[61] A. Klaser, M. Marszalek, and C. Schmid, "A spatio-temporal descriptor based on 3d-gradients," *British Machine Vision Conference (BMVC)*, 2008.

[62] I. Laptev and P. Perez, "Retrieving actions in movie," *IEEE International Conference on Computer Vision (ICCV)*, 2007.

[63] C. Tomasi and R. Manduchi, "Bilateral filtering for gray and color images," *IEEE International Conference on Computer Vision (ICCV)*, 1998.

[64] R. Kimmel, *Numerical Geometry of Images*. Springer, 2003.

[65] N. Dalal and B. Triggs, "Histogram of oriented gradietns for human detection," *IEEE Conference on Computer Vision and Pattern Recognition (CVPR)*, 2005.

[66] I. Laptev, M. Marszalek, C. Schmid, and B. Rozenfeld, "Learning realistic human actions from movies," *IEEE Conference on Computer Vision and Pattern Recognition (CVPR)*, 2008.

[67] R. Duda, P. Hart, and D. Stork, *Pattern Classification, 2nd Edition*. New York: John Wiley and Sons Inc, 2000.

[68] Y. Ke and R. Sukthankar, "PCA-SIFT: A more distinctive representation for local image descriptors," *IEEE Conference on Computer Vision and Pattern Recognition (CVPR)*, 2004.

[69] M. Kendall and A. Stuart, "The advanced theory of statistics, volume 2: Inference and relationship," *Griffin, ISBN 0852642156 (Section 31.19)*, 1973.

[70] M. Tatsuoka, *Multivariate Analysis*. Macmillan, 1988.

[71] T. Calinski, M. Krzysko, and W. Wolynski, "A comparison of some tests for determining the number of nonzero canonical correlations," *Communication in Statistics, Simulation and Computation*, vol. 35, pp. 727–749, 2006.

[72] Y. Benjamini and Y. Hochberg, "Controling the false discovery rate: A practical and powerful approach to multiple testing," *Journal of the Royal Statistical Society. Series B*, vol. 57, no. 1, pp. 289–300, 1995.

[73] F. Devernay, "A non-maxima suppression method for edge detection with sub-pixel accuracy," *Technical report, INRIA*, no. RR-2724, 1995.

[74] N. Petkov and E. Subramanian, "Motion detection, noise reduction, texture suppression and contour enhancement by spatiotemporal gabor filters with surround inhibition," *Biological Cybernetics*, vol. 97, pp. 423–439, 2007.

[75] H. Jhuang, T. Serre, L. Wolf, and T. Poggio, "A biologically inspired system for action recogntion," *IEEE International Conference on Computer Vision(ICCV)*, October 2007.

[76] D. Batra, T. Chen, and R. Sukthankar, "Space-time shapelets for action recogntion," *IEEE Workshop on Motion and video Computing (WMVC)*, January 2008.

[77] Z. Zhang, Y. Hu, S. Chan, and L.-T. Chia, "Motion context: A new representation for human action recognition," *European Conference on Computer Vision (ECCV)*, 2008.

[78] K. Schindler and L. van Gool, "Action snippets: How many frames does human action recognition require," *IEEE Conference on Computer Vision and Pattern Recognition (CVPR)*, 2008.

[79] X. Sun, M. Chen, and A. Hauptmann, "Action recognition via local descriptors and holistic features," *IEEE Conference on Computer Vision and Pattern Recognition (CVPR)*, 2009.

[80] A. Fathi and G. Mori, "Action recognition by learning mid-level motion features," *IEEE Conference on Computer Vision and Pattern Recognition (CVPR)*, 2008.

[81] M. Bregonzio, S. Gong, and T. Xiang, "Recognising actions as clouds of space-time interest points," *IEEE Conference on Computer Vision and Pattern Recognition (CVPR)*, 2009.

[82] J. Liu and M. Shah, "Learning human actions via information maximization," *IEEE Conference on Computer Vision and Pattern Recognition (CVPR)*, 2008.

[83] P. Dollar, V. Rabaud, G. Cottrell, and S. Belongie, "Behavior recognition via sparse spatio-temporal features," *In proceeding of Visual Surveillance and Performance Evaluation of Tracking and Surveillance (VS-PETS)*, October 2005.

[84] A. Wong and J. Orchard, "A nonlocal-means approach to examplar-based inpainting," *IEEE International Conference on Image Processing*, 2008.

[85] K. Rapantzikos, Y. Avrithis, and S. Kollias, "Dense saliency-based spationtemporal feature points for action recognition," *IEEE Conference on Computer Vision and Pattern Recognition (CVPR)*, 2009.

[86] A. Bandopadhay and J. Fu, "Searching parameter spaces with noisy linear constraints," *IEEE Conference on Computer Vision and Pattern Recognition (CVPR)*, 1988.

[87] G. Medioni, I. Cohen, F. Bremond, S. Hongeng, and R. Nevatia, "Event detection and analysis from video streams," *IEEE Transactions on Pattern Analysis and Machine Intelligence (PAMI)*, vol. 23, no. 8, pp. 873–890, August 2001.

[88] T. Veit, F. Cao, and P. Bouthemy, "Probabilistic parameter-free motion detection," *IEEE Conference on Computer Vision and Pattern Recognition (CVPR)*, June 2004.

[89] M. Marszalek, I. Laptev, and C. Schmid, "Actions in context," *IEEE Conference on Computer Vision and Pattern Recognition (CVPR)*, 2009.

[90] S. K. Divvala, D. Hoiem, J. H. Hays, A. Efros, and M. Hebert, "An empirical study of context in object detection," *IEEE Conference on Computer Vision and Pattern Recognition (CVPR)*, 2008.

[91] A. Oliva and A. Torralba, "The role of context in object recognition," *Trends Cognitive Science*, November 2007.

[92] H. Wang, M. M. Ullah, A. Klser, I. Laptev, and C. Schmid, "Evaluation of local spatio-temporal features for action recognition," *British Machine Vision Conference (BMVC)*, 2009.

[93] L. Wolf, T. Hassner, and Y. Taigman, "The one-shot similarity kernel," in *IEEE International Conference on Computer Vision (ICCV)*, 2009.

[94] ——, "Descriptor based methods in the wild," in *Faces in Real-Life Image Workshop in European Conference on Computer Vision (ECCV)*, 2008.

[95] J. Yang, K. Yu, Y. Gong, and T. Huang, "Linear spatial pyramid matching using sparse coding for image classification," in *IEEE Conference on Computer Vision and Pattern Recognition(CVPR)*, 2009.

[96] H. Lee, A. Battle, R. Raina, and A. Y. Ng, "Efficient sparse coding algorithms," in *NIPS*, 2006.

[97] N. Kumar, L. Zhang, and S. K. Nayar, "What is a good nearest neighbors algorithm for finding similar patches in images," *In Proc. European Conference Computer Vision (ECCV)*, 2008.

[98] B. Kulis and K. Grauman, "Kernelized locality-sensitive hashing for scalable image search," *IEEE International Conference on Computer Vision (ICCV)*, 2009.

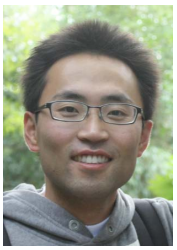

Hae Jong Seo received the B.S. degree and M.S. degree in electrical engineering from Sungkyunkwan University, Seoul, Korea in 2005 and 2006, respectively. He is currently pursuing the Ph.D. degree in electrical engineering at UCSC. His research interests are in the domain of image processing (denoising, interpolation, deblurring, and super-resolution) and computer vision (visual object recognition)

Peyman Milanfar (SM'98) received the BS degree in electrical engineering and mathematics from the University of California, Berkeley, in 1988, and the MS, EE, and PhD degrees in electrical engineering from the Massachusetts Institute of Technology, Cambridge, in 1990, 1992, and 1993, respectively. Until 1999, he was a senior research engineer at SRI International, Menlo Park, California. He is currently a professor of electrical engineering at the University of California, Santa Cruz. He was a consulting assistant professor of computer science at Stanford University, California, from 1998 to 2000, where he was also a visiting associate professor in 2002. His technical interests include statistical signal and image processing and inverse problems. He won a US National Science Foundation CAREER award. He is an associate editor for the IEEE Transaction on Image Processing and was an associate editor for the IEEE Signal Processing Letters from 1998 to 2001. He is a member of the Signal Processing Societys Image, Video, and Multidimensional Signal Processing (IVMSP) Technical Committee. He is a fellow of the IEEE